IET Signal Processing

Review Article

IET Journals
The Institution of Engineering and Technology

S-transform: from main concepts to some power quality applications

ISSN 1751-9675
Received on 23rd January 2019
Revised 31st October 2019
Accepted on 13th December 2019
E-First on 30th January 2020
doi: 10.1049/iet-spr.2019.0042
www.ietdl.org

Carlos Beuter[1] ✉, *Mario Oleskovicz*[1]

[1]*Department of Electrical and Computer Engineering, University of São Paulo – USP, São Carlos School of Engineering – EESC, Avenida Trabalhador São-carlense, 400, CEP 13566-590 – São Carlos – SP, Brazil*

✉ *E-mail: cbeuter@usp.br*

Abstract: Among various spectral analysis tools arisen in the last years, some were more prominent, such as Fourier transform, windowed Fourier transform and wavelet transform (WT). Nevertheless, all of them present implementation restrictions for an ideal extraction for low as well as high frequencies, of variant signals in time, as, for example, signals containing time-varying harmonics. In this sense, this study presents a review of concepts on the S-transform (ST), also known as Stockwell transform, applied in the analysis of some signals in the context of power quality (PQ). ST gathers, in a single function, positive qualities of both short time Fourier transform (STFT) and WT. This study presents a mathematical basis and some considerations regarding ST, referring to published papers, including a comparison between ST and STFT, as well as WT. It is worth emphasising that a final solution for the extraction of the low- and high-frequency information from time-varying signals is not yet available. ST is a satisfactory approach, but it still needs more detailed studies. This study presents a necessary set of steps for a better understanding of ST, reproduction of examples found in correspondent literature, as well as the ones regarding PQ.

Nomenclature

f	frequency, Hz
$g[m, n]$	Gaussian window on time
$G[m, n]$	Gaussian window on frequency
$h(t)$	signal on time
$h[kT]$	discrete time series
H	signal on frequency
j	imaginary part
p, m, q, k	factors that control window
$m\Delta_F$	sample frequency interval
$n\Delta_T$	sample time interval
N	signal length
X	FFT of signal x
ω, w	modified Gaussian window
S	S-transform result
T	time interval, s
t	time, s
$x(t)$	signal on time
X	signal on frequency
α	frequency location
β	frequency bandwidth
ν	frequency variable centre of a band frequency
π	Pi number $\simeq 3.1416$
σ	standard deviation
τ	time location, s

1 Introduction

The search for the optimum representation of the frequency spectrum has become more important along the years, especially nowadays, in the context of power quality (PQ). The need for characterising the phasors that represent harmonic contents has increased with time-varying harmonic (TVH), considering the real non-periodic signal characteristic along time.

Research studies for tools that respond better to TVHs have improved over the years, focusing on higher speed and resolution. Finding an adequate tool, considering PQ challenges, is of vital importance, especially with the proliferation of devices that generate harmonic, interharmonic, and sub/supraharmonic components.

According to the initial research studies, the extraction of the frequency spectrum received its first impulse after investigations on the periodic function decomposition in convergent trigonometric series [1]. Consequently, the Fourier transform (FT) has become one of the widely used tools for obtaining spectral components. However, one of its limitations is the detection and analysis of signals with frequencies that vary over time, which, for some practical applications, may be essential. In 1946, Dennis Gabor proposed a solution for such limitation through windowed use of FT to analyse time–frequency. This was the reason for the emergence of the short time Fourier transform (STFT), also known as windowed Fourier transform (WFT) [2], or as Gabor transform [3]. Nevertheless, the latter is also incapable of adequately trace dynamic signals due to limitations on its fixed time window width. Therefore, the main disadvantages of STFT are the disability to detect and analyse low frequencies and incorrect time resolution of high-frequency events.

Grossmann and Morlet [4] proposed, in 1984, the wavelet transform (WT), which enabled to extract information in time and frequency domains and became the most adequate tool for dynamic signals. However, WT is noise sensible and has limitations in direct intuitive visual interpretation of the frequency scale. Finally, Stockwell *et al*. [5], in 1996, proposed the S-transform (ST). Among ST properties, the most prominent are its resolution, depending on frequency and the time–frequency domain, as well as the extraction of phases that compose the analysed signal.

With the description of generalised S-transform (GST) [6], it was possible to improve the resolution in time on the initial moment and the frequency resolution on the final part of an event. According to the specific analysis, it is possible to apply a different window to ST, as, for example, bi-Gaussian and hyperbolic window, inter alia [7], aiming at a better resolution.

The main problem that drives much of the research previously presented is the restrictions observed by FT, WFT and WT in extracting low- and high-frequency information from time-varying signals, such as, in the context of PQ, signals that contain harmonics varying in time. In this sense, this paper presents a review of concepts on the ST, also known as Stockwell transform, applied in the analysis of some signals in the context of PQ. This paper reviews the ST fundamental mathematical formulation, its properties, as well as results of simulations with ST and other

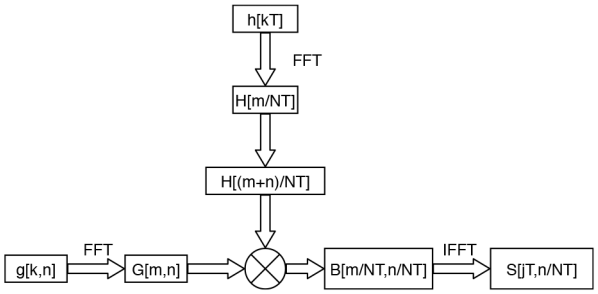

Fig. 1 *Schematic diagram for ST application [10]*

implemented time–frequency analyses, based on correlated literature. It also presents additional topics related to discrete S-transform (DST) and discrete orthonormal Stockwell transform (DOST). A section will be dedicated to GST and its implication in different windowing, with figures of their properties. In addition, some PQ applications will be presented, as well as a brief analysis of their potentialities. It is worth emphasising that a final solution for the extraction of the low- and high-frequency information from time-varying signals is not yet available. ST is a satisfactory approach, but it still needs more detailed studies.

2 S-transform

ST can be considered a hybrid method, between STFT and WT. This tool can be classified as a frequency-dependent STFT or a WT with corrected phase. ST can be defined as

$$S(\tau, f) = \int_{-\infty}^{+\infty} h(t) \underbrace{\frac{|f|}{\sqrt{2\pi}} \mathrm{e}^{-(\tau - t)^2 f^2/2}}_{\text{window}} \mathrm{e}^{-\mathrm{j}2\pi f t}\, \mathrm{d}t\,. \tag{1}$$

The frequency-dependent window enables a frequency resolution with narrower ranges for higher frequencies and wider range ones for lower frequencies. The concentration of the energy resulting from a signal, when analysed by ST and STFT, allows a better comparison of the resulting energies in the time–frequency axes, as subsequently shown. Opposite to WT, phase information provided by ST is connected to origin in time, using FT as a basis, which is not possible with continuous wavelet transform, where phase information is locally referenced [8, 9].

The following section presents DST, its algorithm on the optimised form, as well as some final comparisons between ST and conventional methods as STFT and Wigner distribution function (WDF).

2.1 Discrete S-transform

Considering $h[kT]$, with $k = 0, 1, \ldots, N-1$, denoting a discrete time series corresponding to $h(t)$, with a sampling time interval T, FT is defined by

$$H\left[\frac{n}{NT}\right] = \frac{1}{N} \sum_{k=0}^{N-1} h[kT] \mathrm{e}^{-\mathrm{j}2\pi nk/N}\,. \tag{2}$$

Using (2), TS (1) discrete time series $h[kT]$ is found by alternating $f \to n/NT$ and $\tau \to \mathrm{j}T$:

$$S\left[\mathrm{j}T, \frac{n}{NT}\right] = \sum_{k=0}^{N-1} H\left[\frac{m+n}{NT}\right] \times \mathrm{e}^{-2\pi^2 m^2/n^2} \mathrm{e}^{\mathrm{j}2\pi m\mathrm{j}/N}, \quad n \neq 0 \tag{3}$$

where j,m and $n = 1, \ldots, N-1$. With $n = 0$, ST equals the constant, defined as:

$$S[\mathrm{j}T, 0] = \frac{1}{N} \sum_{m=0}^{N-1} h\left(\frac{m}{NT}\right). \tag{4}$$

Equation (4) creates an average time constant on the zero frequency ($n = 0$), providing that the reverse is exact. *ST* reverse is then

$$h[kT] = \sum_{k=0}^{N-1} \left\{ \frac{1}{N} \sum_{k=0}^{N-1} S\left[\mathrm{j}T, \frac{n}{NT}\right] \right\} \mathrm{e}^{\mathrm{j}2\pi nk/N}\,. \tag{5}$$

Using the fast Fourier transform (FFT) speed would be an alternative to streamline the DST calculation. By definition, ST can be expressed as the convolution of $(x(\tau)\mathrm{e}^{-\mathrm{j}2\pi f\tau})$ and $(|f|\mathrm{e}^{-\pi t^2 f^2})$ (1).

Applying FT to both sides $(x(\tau)\mathrm{e}^{-\mathrm{j}2\pi f\tau})$ and $(|f|\mathrm{e}^{-\pi t^2 f^2})$ the result is

$$S_x(t, f) = \int_{-\infty}^{\infty} X(f + \alpha) \mathrm{e}^{-\pi\alpha^2/f^2} \mathrm{e}^{\mathrm{j}2\pi\alpha t}\, \mathrm{d}\alpha\,. \tag{6}$$

Therefore, DST may be derived from the FFT product of $X(f + \alpha)$ with the windowing $\mathrm{e}^{-\pi\alpha^2/f^2}$ and, finally, applying FFT reverse of $\mathrm{e}^{\mathrm{j}2\pi\alpha t}$.

Considering the sampling interval $t = n\Delta_T$, $f = m\Delta_F$, $\alpha = p\Delta_F$, Δ_T and the sampling frequency Δ_F, DST sampling frequency may be expressed as

$$S_x(n\Delta_T, m\Delta_F) = \sum_{p=0}^{N-1} X[(p+m)\Delta_F] \mathrm{e}^{-\pi(p^2/m^2)} \mathrm{e}^{\mathrm{j}2pn/N}\,. \tag{7}$$

Based on (7), it is possible to obtain the optimised algorithm for ST calculation, as per the next section.

2.2 DST algorithm

Utilising FFT algorithm may streamline ST implementation, given the existing relation between ST and FT, as pointed out in (6). According to the algorithm, the FT of any input signal needs to be calculated only once. Therefore, by using ST on its discrete form, for each required value of frequency m, the spectrum can be moved towards the frequency by m. Gaussian window $G[n, m]$ can then be evaluated and ST calculated using the inverse fast Fourier transform (IFFT), as presented in (7). The algorithm that calculates the ST may be presented as follows [10]:

1. Execute discrete Fourier transform of time series $h[kT]$ (with N samples and a sampling interval T) to obtain $H[m]$ using the FFT routine. This step is calculated once.
2. From the Gaussian on time $g[k, n]$, calculate the Gaussian location $G[n, m]$ for the necessary frequency n/NT.
3. Change the spectrum $H[m/NT]$ to $H[(m + n)/NT]$ for the frequency n/NT.
4. Multiply $H[(m + n)/NT]$ by $G[n, m]$ to obtain $B[n/NT, m/NT]$.
5. Calculate the IFFT of $B[NTn, NTm]$ to obtain the line of $S[NTn, uT]$ corresponding to the frequency m/NT.
6. Repeat steps 3–5 until all lines of $S[n/NT, uT]$ corresponding to all discrete frequencies n/NT are defined.

Fig. 1 shows a schematic representation of this algorithm.

2.3 Discret orthonormal Stockwell transform

In 2007, Stockwell [11] presented an even more efficient alternative to calculate ST, in relation to the initially proposed discrete method (3), called DOST, which utilises an orthogonal set of base functions to locate the spectrum, keeping the local phase properties.

Once the ST phase properties are kept, it is possible to make a cross-spectral analysis to measure phase deviations between each of the multiple components of two-time series as a time–frequency function. Moreover, it is possible to define a generalised instantaneous frequency, applicable to non-stationary broadband signals.

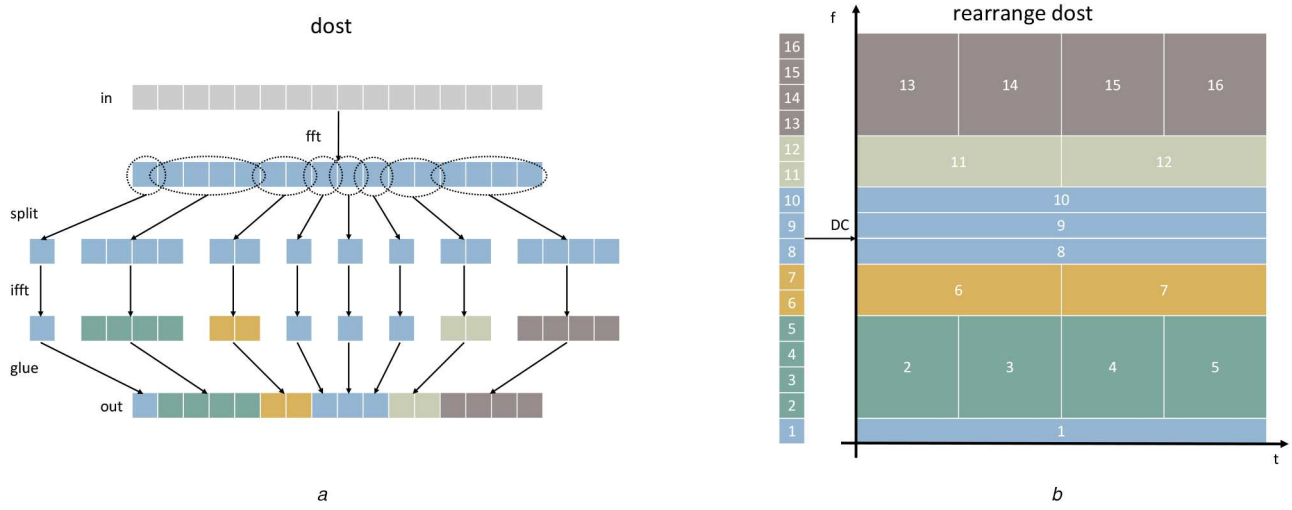

Fig. 2 *DOST diagram proposed*
(a) Processing, ***(b)*** The order of the coefficients into a vector [13]

An example of DOST process gain was presented in [12], in the analysis of PQ-related disturbances, where ST computational processing for a voltage signal of 250 ms spent ∼50 s and used 1 GB of memory, while the DOST computational processing for the same signal spent only 0.03 s and used 124kB of memory.

An efficient ST representation may be defined by the internal sums between a time series $x[kT]$ and the base functions defined as a function of such sums, with the parameters ν (frequency variable indicator of the centre of a band frequency), β (indicator of the frequency bandwidth) and τ (time variable indicator of time location) [11]:

$$Sx[kT] = S\left(\tau T, \frac{f}{NT}\right) = \sum_{k=0}^{k=N-1} h[kT] S_{[\nu,\beta,\tau]}[kT]\,. \tag{8}$$

Base function $S_{[\nu,\beta,\tau]}[kT]$ is written as

$$S_{[\nu,\beta,\tau]}[kT] = \frac{1}{\sqrt{\beta}} \sum_{f=\nu-\beta/2}^{f=\nu+\beta/2-1} \mathrm{e}^{\mathrm{i}2\pi(k/N)f} \times \mathrm{e}^{-\mathrm{i}2\pi(\tau/\beta)f} \mathrm{e}^{-\mathrm{i}2\pi(N/2NT)\tau T}\,. \tag{9}$$

$1/\sqrt{\beta}$ is a normalisation factor to provide the orthonormality of base functions. Therefore, base functions for DOST in ν frequency, β and time index τ may be given as:

$$S_{[\nu,\beta,\tau]}[kT] = \frac{\mathrm{i}\mathrm{e}^{\mathrm{i}\pi\tau}}{\sqrt{\beta}} \sum_{f=\nu-\beta/2}^{f=\nu+\beta/2-1} \mathrm{e}^{\mathrm{i}2\pi((k/N)-(\tau/B))f}\,. \tag{10}$$

Fig. 2*a* shows the DOST processing diagram proposed by Battisti and Riba [13]. The diagram indicates that the sampled signal (in) passes into the frequency domain (fft), where it is then split by larger or smaller clusters, depending on the position of the frequency bandwidth (called 'frequency bandwidth decomposition of the DOST' by the authors), as proposed by (8)–(10), whose inverse (ifft) is re-clustered (glue) in a linear output (out).

Fig. 2*b* indicates that the linear output can be visualised by a rearrangement along the time–frequency axis of the energy coefficients. At this point, a 'mirrored' representation occurs for the positive side (lines 10–16) as well as for the negative side (lines 02–08) of the frequency, as well as the central output $f = 0$ (DC in lines 1 and 9) [13, 14].

2.4 Comparisons

This subsection presents and discusses simulation resultant of [5], indicating time-series classes, for which ST is considerably useful and has a satisfactory performance.

Fig. 3*a* is a time series composed of three distinct frequency variations used to illustrate and compare ST performance in relation to STFT.

A comparison between Figs. 3*b* and *c* shows that ST has a better resolution in frequency than STFT for a 6 Hz frequency. Nevertheless, the ST resolution is worse than STFT for the frequency explosion. By comparison, it is observed that the frequency bandwidth for this ST explosion is between about 45 and 65 Hz (considering $\Delta = 20$ Hz). For the STFT, the frequency bandwidth is 47–60 Hz (with a $\Delta = 13$ Hz), i.e. a smaller bandwidth when compared to ST. Both tools behaved similarly for a 26 Hz frequency. However, by observing temporal resolution, ST can detect the occurrence time and the energy variation on the highest frequency. Furthermore, from Figs. 3*c* and *d*, STFT has a commitment between detecting short-length high- and low-frequency signals. When the STFT window width is widened, it demonstrates a low capacity to distinguish the three signal components.

Similarly, Fig. 4*a* presents a time series composed of two blasts on the 107.52 Hz frequency and two crossed chirps. From Fig. 4*b*, ST may detect all four components. In Fig. 4*c*, STFT can only detect the chirps, but it cannot detect the blasts in higher frequencies. In Fig. 4*d* WDF result is presented, where a good resolution in time and frequency for the crossed chirps is observable. The disadvantage, though, is that WDF has crossed terms that will produce too many undesired values (lines) represented by the noise. Furthermore, crossed terms will make both blasts distorted.

An implementation of the fast algorithm for DOST ($\mathcal{O}(N \log N)$) presented in [11, 14–16] is mathematically described by Battisti and Riba [13]. Fig. 3*a* illustrates the DOST application result for the same synthetic signal presented in Fig. 5*b*. Symmetry in relation to the x-axis is not seen in the ST, given in Fig. 3*b*. Although not being visually friendly, orthogonality provides a more efficient representation through orthogonal functions, aiming not only at higher processing speed but also at the complete recovery of the original signal. These characteristics could, for example, be studied in the context of the research presented by Reddy *et al*. [12], which may result in a promising application in the compression and decompression of signals in PQ [17].

3 Different Gaussian window controls

This section presents some proposals to control the Gaussian window width. The first of them was the GST [18] that, in its turn, originated various others, such as modified S-transform (MST) [19], bi-Gaussian S-transform (BGST) [20] and variations, as presented below.

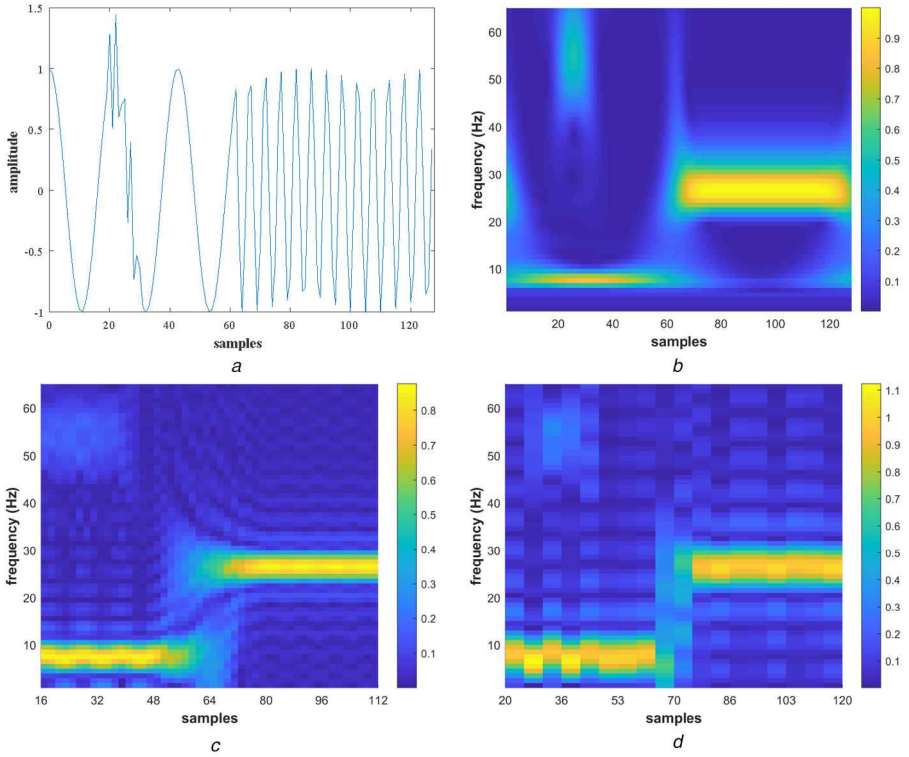

Fig. 3 *Performance comparison with*

(a) Time series with 127 samples composed of three different synthetic signals. The first half presents a 6 Hz frequency, whereas second half presents a 25 Hz frequency and an explosion signal for t equal to 20 s with 52 Hz. The function that defines the samples is given by $h[0{:}63] = \cos(2\pi t * 6.0/128.)$, $h[63{:}127] = \cos(2\pi * 25.0/128)$, $h[20{:}30] = h[20{:}30] + 0.5 * \cos(2\pi t * 52.0/128.0)$, ***(b)*** ST amplitude for the time series of part (a), ***(c)*** STFT for time series of (a) using a Gaussian window, with a standard deviation of 16 units, ***(d)*** the same as in (c), yet altering window size to 20 units and the form to a rectangular window. Reproduced based on [5]

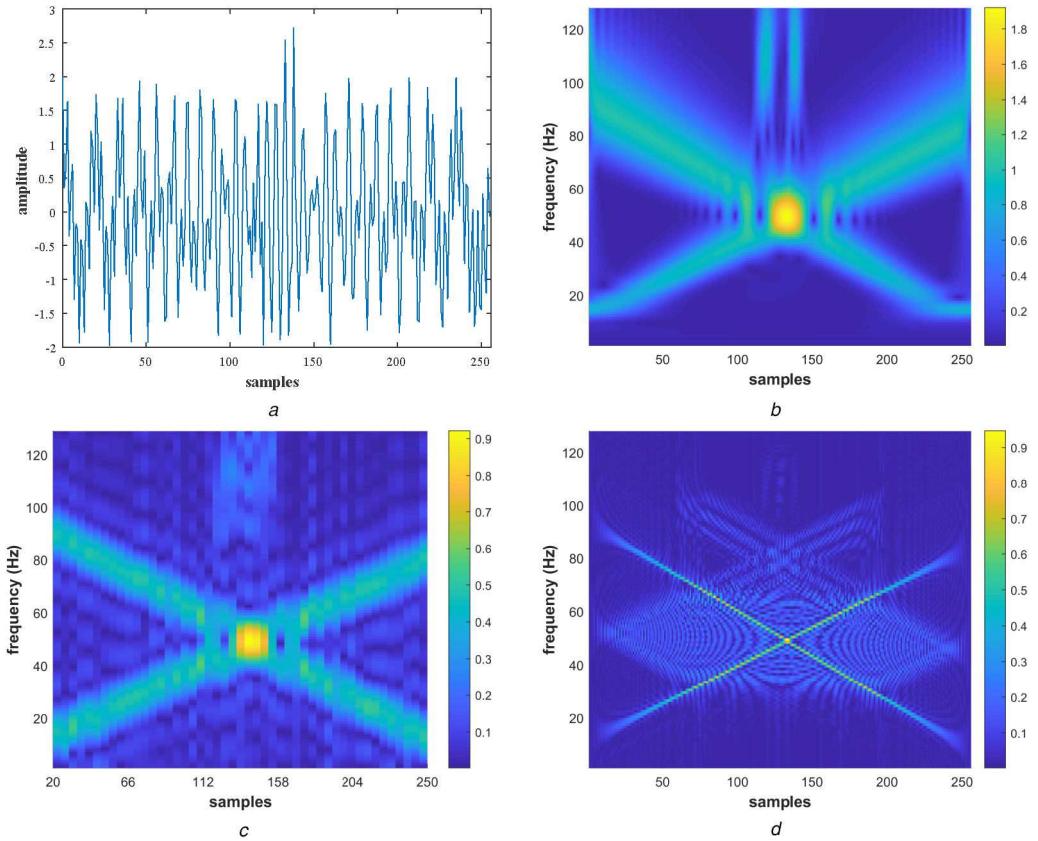

Fig. 4 *Performance comparison with*

(a) Synthetic time series composed by two blasts of 107.52 Hz frequency and two crossed chirps, according to the following expression: $h[0{:}255] = \cos(2\pi(10 + t/7) * t/256) + \cos 2\pi(256/2.8 - t/6.0) * t/256)$, $h[114{:}122] = h[114{:}122] + \cos(2\pi t * 0.42)$ and $h[134{:}142] = h[134{:}142] + \cos(2\pi t * 0.42)$, ***(b)*** ST amplitude of (a) time series, ***(c)*** STFT amplitude (with Gaussian window) of time series in (a), ***(d)*** WDF of (a) time series [5]

3.1 Generalised S-transform

GST is defined in [18] as

$$S_h^{\boldsymbol{p}}(\tau, f) = \int_{-\infty}^{+\infty} h(t)\omega^{\boldsymbol{p}}(\tau - t, f)\mathrm{e}^{-\mathrm{j}2\pi f t}\,\mathrm{d}t, \tag{11}$$

where $\boldsymbol{p}$ is a set of parameters that determines the w form and property, which is the ST window as in the equation:

$$\omega^{\boldsymbol{p}}(t - \tau, f) = \frac{|f|}{\sqrt{2\pi}\,.\,\boldsymbol{p}}\mathrm{e}^{-(t-\tau)^2 f^2/2\boldsymbol{p}^2}. \tag{12}$$

GST is, then, obtainable through FT:

$$S^p(\tau, f) = \int_{-\infty}^{+\infty} H(\alpha + f)W^p(\alpha, f)\mathrm{e}^{\mathrm{j}2\pi\alpha\tau}\,\mathrm{d}\alpha, \tag{13}$$

where,

$$H(\alpha + f) = \int_{-\infty}^{+\infty} h(t)\mathrm{e}^{\mathrm{j}2\pi(\alpha+f)t}\,\mathrm{d}t, \tag{14}$$

and

$$W^p(\alpha, f) = \int_{-\infty}^{+\infty} w^p(t, f)\mathrm{e}^{-\mathrm{j}2\pi\alpha t}\,\mathrm{d}t\,. \tag{15}$$

ST w window ought to satisfy four conditions [20]:

$$\int_{-\infty}^{+\infty} \Re\{\omega^p(\tau, f)\}\,\mathrm{d}\tau = 1, \tag{16}$$

$$\int_{-\infty}^{+\infty} \Im\{\omega^p(\tau, f)\}\,\mathrm{d}\tau = 0, \tag{17}$$

$$\omega^p(\tau - t, f) = [\omega^p(\tau - t, -f)]^*, \tag{18}$$

$$\frac{\partial}{\partial t}\Phi^p(\tau - t, f)\big|_{t=\tau} = 0. \tag{19}$$

The highlights are the first condition (16) that provides ST convergence to FT:

$$\int_{-\infty}^{+\infty} S^p(\tau, f)\,\mathrm{d}\tau = H(f), \tag{20}$$

once integrated to the whole τ, and the third condition (18) that provides symmetry between the function forms analysed in ST, either for positive or negative frequencies.

Based on this generalisation and utilising the described p parameter, some ST variation proposals arose, aiming at a better representation of frequency along the time axis, as the MST and BGST, described below.

3.2 Modified S-transform

One of the ways to control the Gaussian window is to vary linearly the window standard deviation with the frequency, through a progressive width control, given by the following relation:

$$\boldsymbol{p} = mf, \tag{21}$$

as discussed in [10]. Nevertheless, in order to better use this control artifice [19], a k factor is also added:

$$\boldsymbol{p} = mf + k, \tag{22}$$

which applied to the ST results in a variant of (12):

$$\omega^{m,k}(t - \tau, f) = \frac{|f|}{\sqrt{2\pi}\cdot(mf + k)}\mathrm{e}^{-(t-\tau)^2 f^2/2(mf+k)^2}. \tag{23}$$

The final expression is similar to the one presented in (11):

$$S_h^{m,k}(\tau, f) = \int_{-\infty}^{+\infty} h(t)\cdot w^{(m,k)}(t, f)\cdot \mathrm{e}^{-\mathrm{i}2\pi f t}\,\mathrm{d}t\,. \tag{24}$$

Parcel

$$\frac{|f|}{(mf + k)}, \tag{25}$$

represents the number of cycles (periods) of a frequency that may be contained in a standard deviation σ of the Gaussian window. So, $\sigma(f)$ provides an improved and progressive resolution in this case [19]. When too small, the Gaussian window retains few cycles from the sine wave and the frequency resolution degrades in low frequencies. Conversely, if the window is too big, it retains more cycles inside itself and, as consequence, time resolution degrades in high frequencies [19].

3.3 Other windowing proposals

Another variation proposed by Sejdić *et al*. [21] was controlling the Gaussian window width through the equation

$$\boldsymbol{p} = \frac{1}{|f|^q}. \tag{26}$$

Therefore, the ST related to p parameter may be calculated as

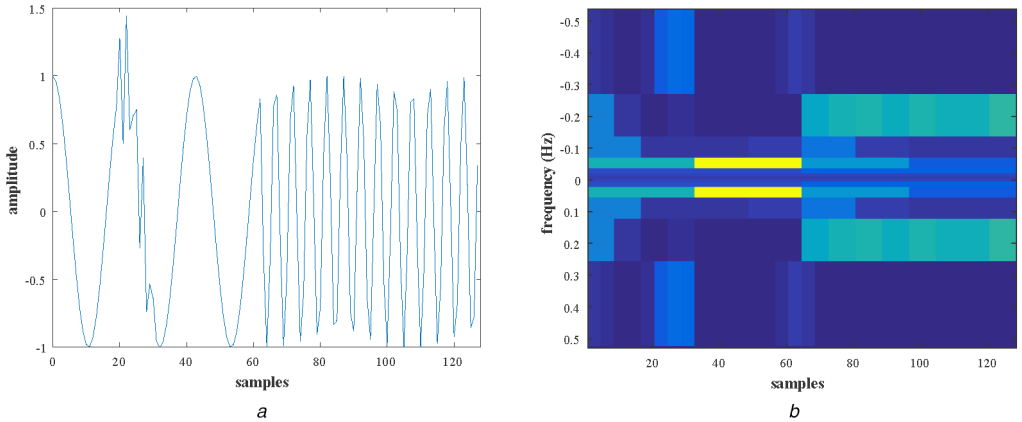

a *b*

Fig. 5 *Signal and DOST results, where*
(a) Time series was defined and presented in Fig. 3*a*, ***(b)*** Representation of DOST the synthetic signal presented in *(a)*

$$S_x^q(\tau, f) = \int_{-\infty}^{+\infty} x(t) \frac{|f|^q}{\sqrt{2\pi}} \cdot \mathrm{e}^{-t^2 f^2/2 f^{2q}}. \quad (27)$$

Moreover, a combined proposal following (22) introduced a new arrangement for parameter q [19]:

$$\boldsymbol{p} = m f^q + k. \quad (28)$$

Similarly to the modified Gaussian window (23), this may be represented by

$$w^{m,q,k}(\tau - t, f) = \frac{|f|}{\sqrt{2\pi}(m f^q + k)} \cdot \mathrm{e}^{-(t-\tau)^2 f^2/2(m f^q + k)^2}, \quad (29)$$

whose final expression is similar to (24).

In all variations, when $\boldsymbol{p} = 1$ or $m = 1$, $q = 1$ and $k = 0$, it is possible to return the original equation (1).

Still, other proposals have come up with differentiated solutions, such as [22] with a compact support kernel.

4 Optimisation by maximum energy concentration

As seen in Section 3, there are various ways to control the Gaussian window width. It is more challenging when various parameters are involved, as presented in (28) with variables m, q and k. In [19], for example, the authors empirically selected such parameters. Nevertheless, these cannot be generalised for all kinds of signals. It would then be more adequate to generate such parameters adaptively, according to the nature of the signal. In this sense, Sejdić *et al*. [21] proposed the use of the genetic algorithm (GA) to select m, q and k, obtaining the transform with the highest energy concentration, indicated by the best GA selection.

Concentration measure (CM), using ST, is obtainable by the equation below:

$$\mathrm{CM}(m, q, k) = \frac{1}{\int_{-\infty}^{+\infty} \int_{-\infty}^{+\infty} \left| \overline{S_x^{m,q,k}}(t, f) \right| \mathrm{d}t \, \mathrm{d}f}, \quad (30)$$

where

$$\overline{S_x^{m,q,k}}(t, f) = \frac{S_x^{m,p,k}(t, f)}{\sqrt{\int_{-\infty}^{+\infty} \int_{-\infty}^{+\infty} \left| S_x^{m,q,k}(t, f) \right|^2 \mathrm{d}t \, \mathrm{d}f}}. \quad (31)$$

Optimisation by CM provides a better resolution in frequency along time, particularly the signals that present TVH in their composition.

Following the same idea, Beuter *et al*. [23] proposed an optimised window, by means of a variant of particle swarm optimisation (PSO) called adaptive individual inertia weight based on best, worst and individual (AIW-PSO). Some of the presented results indicated additional gains in energy concentration and better resolution on time–frequency representation, as well as the indication of many other solutions of local maximums that serve the highest CM.

5 Power quality applications

In the PQ field, manifested disturbances may be classified by voltage variations of short (sags, swells and interruptions) and long (undervoltage, overvoltage and sustained interruptions) duration, oscillatory and impulsive transients, as well as waveform distortions (harmonic, interharmonic, noise, notching and direct current (DC) component), inter alia. In this context, Dash *et al*. [24] may be considered as one of the first works approaching ST implementation in PQ.

In order to have a better overview of the context in PQ, this research reproduces a comparison of analyses resulting from ST and WT application to signals that characterise problems of voltage sag and swell, transitory oscillatory, harmonic distortions and noise, as presented in [25]. It is worth mentioning that the authors

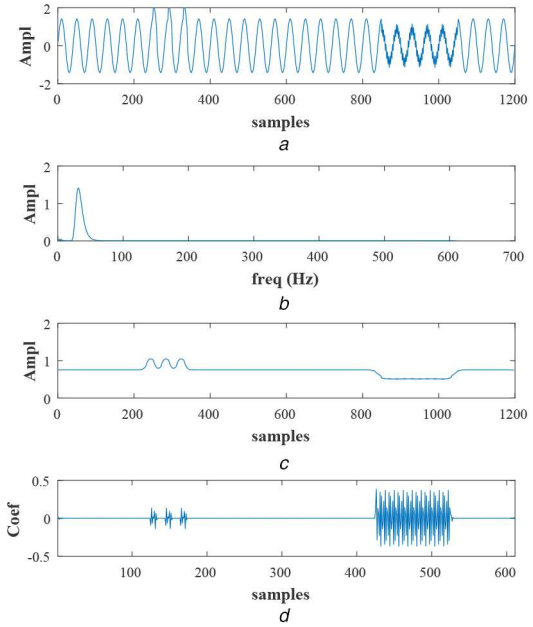

Fig. 6 *Synthetic signals with voltage swell and sag with 30 dB noise superposition [25]*
(a) Oscillogram, ***(b)*** Spectrogram, ***(c)*** ST, ***(d)*** WT coefficients (db4)

in [24, 26], inter alia, found similar results to the ones presented here and, therefore, follow the same approach principle.

Fig. 6*a* presents a situation of voltage swell and sag, with a superposition of 30 dB noise. Fig. 6*b* is the spectrogram corresponding to the magnitude of frequency components, with a 60 Hz fundamental frequency. Conversely, Fig. 6*c* presents the root mean square (RMS) values of the analysed signal. RMS values are calculated based on the maximum amplitude of the ST resulting matrix for each sample, as found in [25]:

$$\left| S\left[\mathrm{j}T, \frac{n}{NT} \right] \right|. \quad (32)$$

Finally, Fig. 6*d* represents the coefficients that result from WT application using the mother wavelet of the Daubechies family with support 4 (db4).

As observed, solely through the spectrum represented in Fig. 6*b*, it is not possible to obtain much information on synthesised events over time. However, a comparison between Figs. 6*c* and *d* shows a lot of noise in the signal, so that WT was unable to identify manifested sag and swell conditions. ST, in its turn, allows correct detection in time as well as amplitude quantification of sag and swell occurrences, even in the presence of noise.

Fig. 7*a* depicts a synthetic signal with voltage sag and swell in the presence of harmonic distortion. Fig. 7*c* shows that, even in the continuous presence of harmonic distortion, ST is able to clearly detect and classify the occurrence of manifested voltage sag and swell. This is also true, but may be hindered, via WT application (Fig. 7*d*).

Fig. 8*a* represents a voltage signal formed by a sequence of PQ disturbances with a 30 dB noise superimposed. The following sequence forms the signal: steady-state signal set at 60 Hz; initial oscillatory transient; voltage sag; oscillatory transient end; and return to the steady-state signal. In Fig. 8*b* FFT spectral analysis is used as reference. In Fig. 8*c* the analysis resulting from the application of the ST reflected on the time axis is displayed. The spectral analysis indicates noise immunity and displays precisely the beginning and end of each event. The same does not occur with the use of WT in Fig. 8*d*, which is severely affected by the noise superimposed on the signal.

Fig. 9*a* reproduces the steady-state signal (fundamental frequency of 60 Hz) plus 40 dB of noise and a voltage fluctuation from sample 500 (37.5 ms). The spectral scattering, indicating inter-harmonic and sub-harmonic frequencies, characterising the

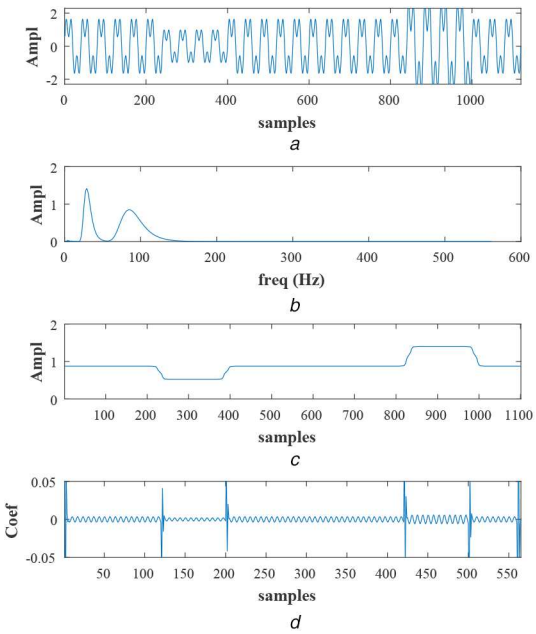

Fig. 7 *Synthetic signals with voltage sag and swell in the presence of harmonic distortion [25]*
(a) Oscillogram, ***(b)*** Spectrogram, ***(c)*** ST, ***(d)*** WT coefficients (db4)

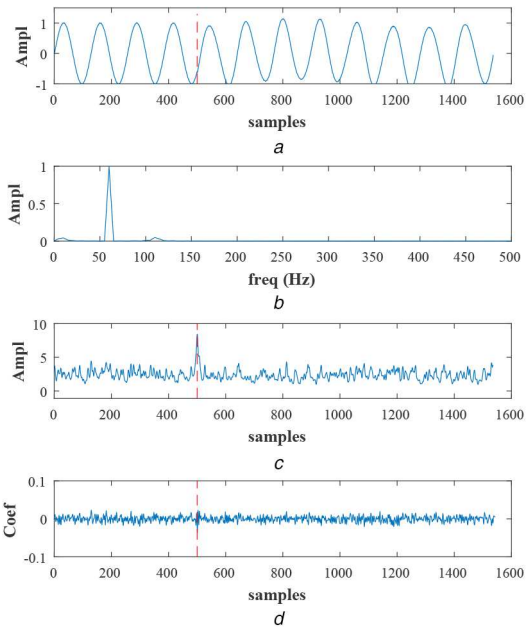

Fig. 9 *Synthetic signals with voltage fluctuation started at 37.5 ms with the superposition of a 40 dB noise. Figure added for this article review*
(a) Oscillogram, ***(b)*** Spectrogram, ***(c)*** ST, ***(d)*** WT coefficients (db4)

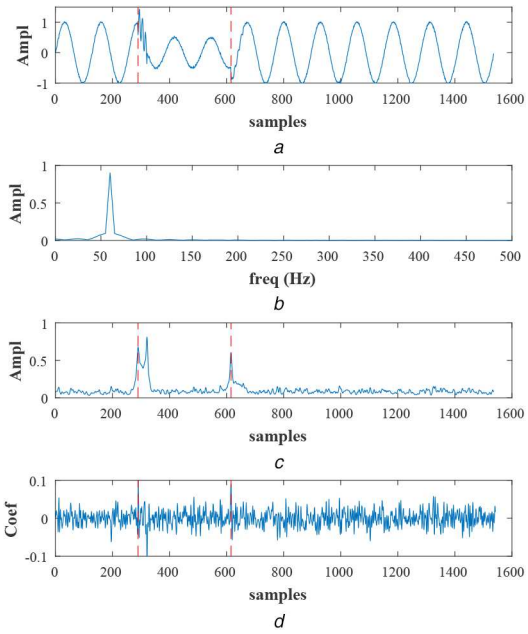

Fig. 8 *Synthetic signals with initial and final oscillatory transients interspersed with a voltage sag and the superposition of 30 dB noise. Figure added for this article review*
(a) Oscillogram, ***(b)*** Spectrogram, ***(c)*** ST, ***(d)*** WT coefficients (db4)

voltage fluctuation, is shown in Fig. 9*b*. The result of the analysis via a ST with relative superimposed noise immunity is presented, allowing to exactly characterise the beginning of the voltage fluctuation event. In Fig. 9*d* it is observed that WT is affected by noise and does not provide information on the beginning of the observed voltage fluctuation.

The authors in [25] pointed out an accuracy above 92% in classifying disturbances associated with the PQ fault even in the presence of a 20 dB noise. However, for a 40 dB noise, the same authors stated a 99% accuracy.

Similarly, other papers use the ST characteristics and properties to classify disturbances, such as [27], or even with other combined techniques, as found in [28–31].

A form of visualisation resulting from the ST in function of the time, when applied to two other random synthetic signals, is presented in Figs. 10*a* and *b*. Signals may be analysed and compared regarding resolution commitment in frequency versus time. Windowing, in the last two examples, was not optimised as the CM presented before.

In the example of Fig. 10*b*, the surface depicted in Fig. 10*c* illustrates ST potentiality for a more detailed examination along time for determinate frequencies, as for 60 Hz in Fig. 10*d*. Even though the waveband is short (two cycles between 30 and 70 ms), frequency variation, if well-explored, may be considered, for example, in some philosophies of digital protection for electrical systems. A computational implementation of optimised ST determines a better representation of analysed signals in the considered time interval. This potentiality was not explored in [27], nor in [25] or other research studies that were consulted up to the present moment.

In Fig. 11*a*, the oscillatory transient is identified by ST through two curves (curves I and II) extending along the frequency axis. Likewise, as pointed out in Fig. 8, this 3D representation indicates that, during the transition between the events, frequencies were around 0.7 kHz.

In Fig. 11*b*, for better visualisation, a magnification was presented in the range 0.2–3.0 kHz. In the transition section of the steady-state signal for the voltage fluctuation, a peak is observed in 65 ms, highlighting the region of the signal with superimposed noise.

Additional examples of ST applications in PQ could be listed as like inrush current detection [32, 33], harmonic detection [34–36], current harmonic distortion analysis and/or voltage [37, 38] and flicker [39, 40].

6 Conclusion

This paper presented the fundamental concepts of ST and its relations to STFT and WT. Visual comparisons with STFT, WT and WDF pointed a better spectral resolution for ST. The GST and its windowed application show that it is possible to establish a relation between the Gaussian windowing due to the frequency and its form (width and amplitude) for different density results in the time–frequency plane.

Therefore, there are different proposals to choose the parameters to form the Gaussian window. An optimised and adequate choice provides a higher energy concentration and, thus, better resolution in time–frequency. For different applications, it is possible to choose an adequate window and to obtain a good resolution according to the desired emphasis.

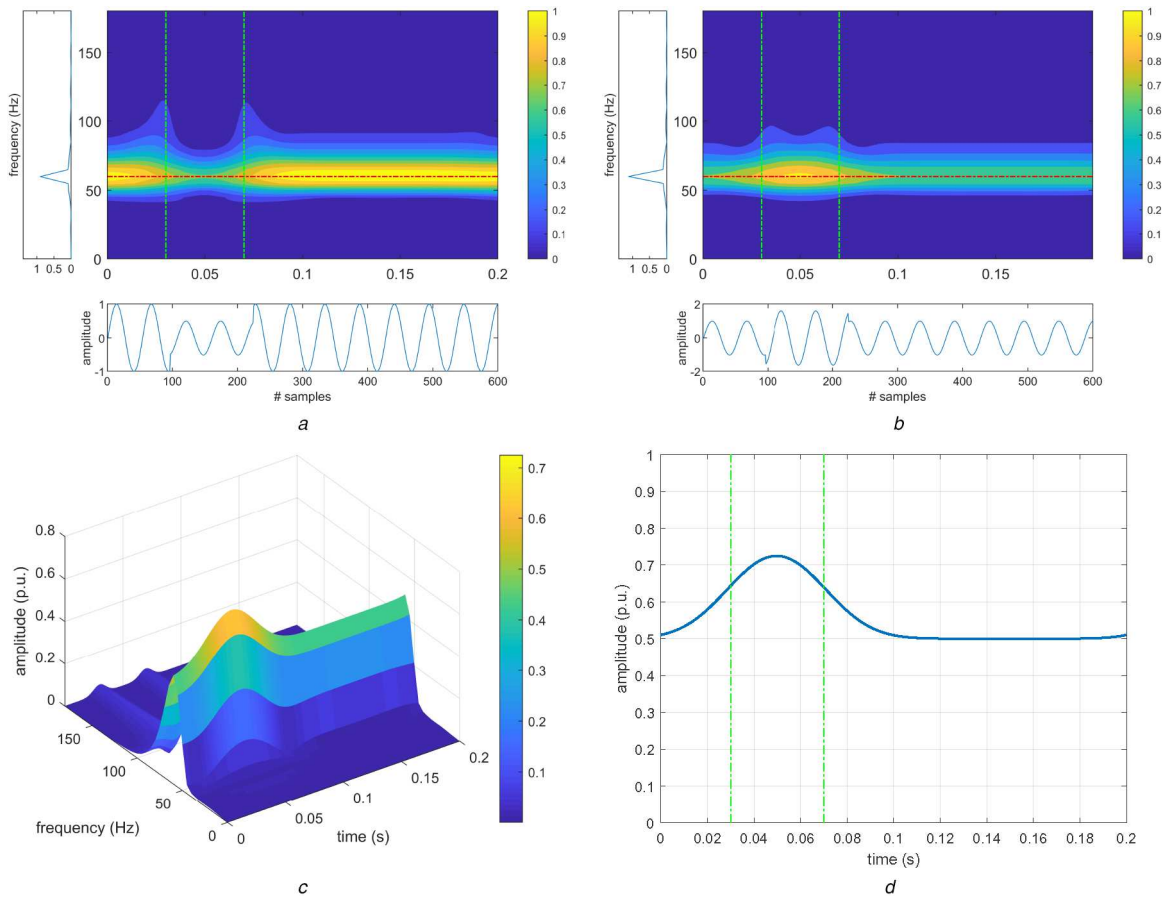

Fig. 10 *Synthetic disturbances generated from a 1 p.u. sinusoidal wave and voltage interruptions between 30 and 70 ms (delimited by green vertical dashed lines), and that are compatible with the horizontal oscillographies. The red horizontal dashed line indicates 60 Hz frequency that is also shown in the frequency spectrum via FFT, put on the left vertical*

(a) 0.5 p.u. sag, ***(b)*** 1.6 p.u. voltage swell, ***(c)*** Surface generated for voltage swell case, ***(d)*** Result, considering only the 60 Hz frequency

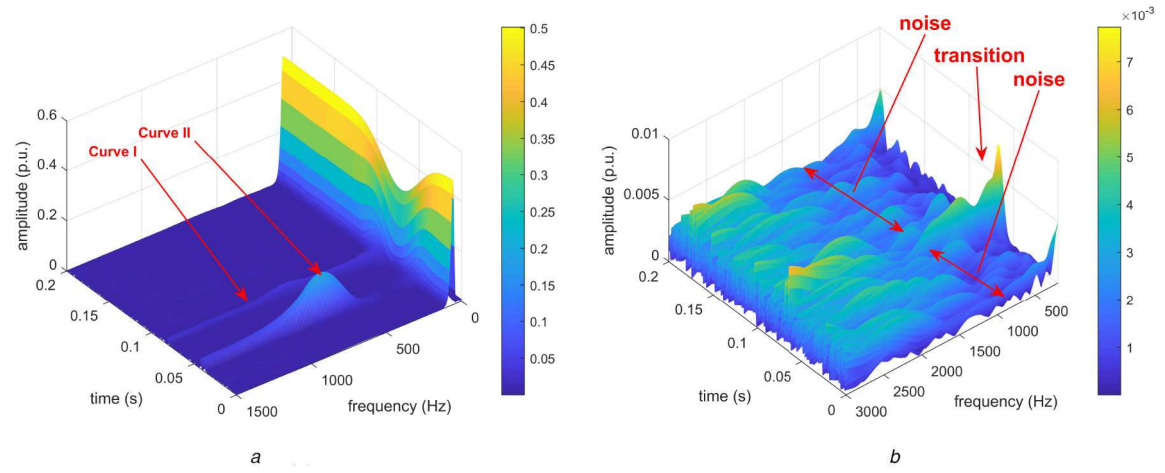

Fig. 11 *ST perspective showing an*

(a) Initial and final oscillatory transients interspersed with a voltage sag in the presence of a 30 dB noise, as shown in Fig. 8, ***(b)*** Signal in the presence of a 40 dB noise and voltage fluctuation started at 37.5 ms, as indicated in Fig. 9

DOST allows higher processing speed, although it is not often visually friendly, exactly because it is synthesised by orthogonal functions. In specific applications, such as image digital processing, DOST is efficient and appropriate.

For analyses in the PQ context, ST was able to identify a disturbance with noise or transitory, where WT was not able to obtain similar results due to noise sensitivity. However, ST still has two disadvantages. The first is related to the DC component of exponential decay (frequency = 0), because it cannot analyse a DC variation in time, considering only the average length of the analysed signal. The second one is associated with high frequencies, where the window is too narrow, which implies a reduced number of signal samples to be analysed by ST. It may compromise frequency–time resolution quality.

7 References

[1] Fourier, J.B.J.: '*Théorie analytique de la chaleur*' (Chez Firmin Didot, père et fils, France, 1822)

[2] Bolzan, M.J.A.: 'Transformada em ondeleta: uma necessidade', *Revista Brasileira de Ensino de Fisica*, 2006, **28**, pp. 563–567. Available at http://dx.doi.org/10.1590/S1806-11172006000400019

[3] Gabor, D.: 'Theory of communication. Part 3: frequency compression and expansion', *J. Inst. Electr. Eng. Part III: Radio Commun. Eng.*, 1946, **93**, (26), pp. 445–457. Available at https://ieeexplore.ieee.org/document/5298523

[4] Grossmann, A., Morlet, J.: 'Decomposition of hardy functions into square integrable wavelets of constant shape', *SIAM J. Math. Anal.*, 1984, **15**, (4), pp. 723–736. Available at https://doi.org/10.1137/0515056

[5] Stockwell, R.G., Mansinha, L., Lowe, R.P.: 'Localization of the complex spectrum: the s transform', *IEEE Trans. Signal Process.*, 1996, **44**, (4), pp. 998–1001. Available at https://doi.org/10.1109/78.492555

[6] Mansinha, L., Stockwell, R.G., Lowe, R.P., *et al.*: 'Local s-spectrum analysis of 1-d and 2-d data', *Phys. Earth Planet. Inter.*, 1997, **103**, (3), pp. 329–336. Available at http://www.sciencedirect.com/science/article/pii/S0031920197000472

[7] Wang, Y.H.: 'The tutorial: S transform', 2010. Available at http://citeseerx.ist.psu.edu/viewdoc/download?doi=10.1.1.694.8727&rep=rep1&type=pdf

[8] Moukadem, A., Ould-Abdeslam, D., Dieterlen, A.: '*Time–frequency analysis: the s-transform*' (John Wiley & Sons, Inc., 2014), pp. 21–59. Available at http://dx.doi.org/10.1002/9781118908686.ch2

[9] Ventosa, S., Simon, C., Schimmel, M., *et al.*: 'The S-transform from a wavelet point of view', *IEEE Trans. Signal Process.*, 2008, **56**, (7), pp. 2771–2780

[10] Sahu, S.S., Panda, G., George, N.V.: 'An improved S-transform for time-frequency analysis'. 2009 IEEE Int. Advance Computing Conf., Patiala, India, 2009, pp. 315–319

[11] Stockwell, R.G.: 'A basis for efficient representation of the s-transform', *Digit. Signal Process.*, 2007, **17**, (1), pp. 371–393. Available at https://doi.org/10.1016/j.dsp.2006.04.006

[12] Reddy, M.J.B., Raghupathy, R.K., Venkatesh, K.P., *et al.*: 'Power quality analysis using discrete orthogonal s-transform (dost)', *Digit. Signal Process.*, 2013, **23**, (2), pp. 616–626. Available at http://www.sciencedirect.com/science/article/pii/S1051200412002321

[13] Battisti, U., Riba, L.: 'Window-dependent bases for efficient representations of the stockwell transform', *Appl. Comput. Harmon. Anal.*, 2016, **40**, (2), pp. 292–320. Available at http://www.sciencedirect.com/science/article/pii/S1063520315000184

[14] Wang, Y.: 'Efficient Stockwell transform with applications to image processing'. PhD thesis, UWSpace, University of Waterloo, 2011. Available at http://hdl.handle.net/10012/5963

[15] Wang, Y., Orchard, J.: 'Fast discrete orthonormal stockwell transform', *SIAM J. Sci. Comput.*, 2009, **31**, (5), pp. 4000–4012. Available at https://doi.org/10.1137/080737113

[16] Brown, R.A., Lauzon, M.L., Frayne, R.: 'A general description of linear time-frequency transforms and formulation of a fast, invertible transform that samples the continuous s-transform spectrum nonredundantly', *IEEE Trans. Signal Process.*, 2010, **58**, (1), pp. 281–290

[17] de Andrade, L.C.M., Nanjundaswamy, T., Oleskovicz, M., *et al.*: 'Advances in classification and compression of power quality signals', *J. Control Autom. Electr. Syst.*, 2019, **30**, (3), pp. 402–412

[18] Pinnegar, C.R., Mansinha, L.: 'Time-local Fourier analysis with a scalable, phase-modulated analyzing function: the s-transform with a complex window', *Signal Process.*, 2004, **84**, (7), pp. 1167–1176. Available at http://dx.doi.org/10.1016/j.sigpro.2004.03.015

[19] Assous, S., Boashash, B.: 'Evaluation of the modified s-transform for time–frequency synchrony analysis and source localisation', *EURASIP J. Adv. Signal Process.*, 2012, **2012**, (1), pp. 49–67. Available at https://doi.org/10.1186/1687-6180-2012-49

[20] Pinnegar, C.R., Mansinha, L.: 'The bi-Gaussian s-transform', *SIAM J. Sci. Comput.*, 2003, **24**, (5), pp. 1678–1692. Available at https://doi.org/10.1137/S1064827500369803

[21] Sejdić, E., Djurović, I., Jiang, J.: 'A window width optimized s-transform', *EURASIP J. Adv. Signal Process.* 2008, **2008**, (1), p. 672941. Available at https://doi.org/10.1155/2008/672941

[22] Zidelmal, Z., Hamil, H., Moukadem, A., *et al.*: 'S-transform based on compact support kernel', *Digit. Signal Process.*, 2017, **62**, pp. 137–149

[23] Beuter, C.H., Oleskovicz, M., Golfieri, C.I., *et al.*: 'Selection of the optimized window for the generalized s-transform using the AIW-PSO algorithm'. 2018 18th Int. Conf. on Harmonics and Quality of Power (ICHQP), Ljubljana, Slovenia, 2018, p. 6. Available at https://doi.org/10.1109/ichqp.2018.8378882

[24] Dash, P.K., Panigrahi, B.K., Panda, G.: 'Power quality analysis using s-transform', *IEEE Trans. Power Deliv.*, 2003, **18**, (2), pp. 406–411. Available at https://doi.org/10.1109/TPWRD.2003.809616

[25] Shi, Z., Ruirui, L., Qun, W., *et al.*: 'The research of power quality analysis based on improved s-transform'. 2009 9th Int. Conf. on Electronic Measurement Instruments, Beijing, People's Republic of China, 2009, pp. 2-477–2-481. Available at https://doi.org/10.1109/ICEMI.2009.5274515

[26] Shicheng, X., Li, X., Leping, B.: 'An effective s-transform feature extraction method for classification of power quality disturbance signals'. 2015 Chinese Automation Congress (CAC), Wuhan, People's Republic of China , 2015, pp. 1555–1560. Available at https://doi.org/10.1109/CAC.2015.7382748

[27] Noh, F.H.M., Rahman, M.A., Yaakub, M.F.: 'Performance of modified s-transform for power quality disturbance detection and classification', *TELKOMNIKA (Telecommun. Comput. Electron. Control)*, 2017, **15**, (4), p. 1520

[28] Biswal, M., Dash, P.K.: 'Detection and characterization of multiple power quality disturbances with a fast s-transform and decision tree based classifier', *Digit. Signal Process.*, 2013, **23**, (4), pp. 1071–1083. Available at http://www.sciencedirect.com/science/article/pii/S1051200413000353

[29] Rodriguez, A., Ruiz, I.E., Aguado, J., *et al.*: 'Classification of power quality disturbances using s-transform and artificial neural networks'. 2011 Int. Conf. on Power Engineering, Energy and Electrical Drives, Malaga, Spain, 2011, pp. 1–6

[30] Zhao, F., Yang, R.: 'Power-quality disturbance recognition using s-transform', *IEEE Trans. Power Deliv.*, 2007, **22**, (2), pp. 944–950

[31] Lee, I.W.C., Dash, P.K.: 'S-transform-based intelligent system for classification of power quality disturbance signals', *IEEE Trans. Ind. Electron.*, 2003, **50**, (4), pp. 800–805

[32] Mokryani, G., Siano, P., Piccolo, A.: 'Detection of inrush current using s-transform and competitive neural network'. 2010 12th Int. Conf. on Optimization of Electrical and Electronic Equipment, Basov, Romania, 2010, pp. 191–196

[33] Sendilkumar, S., Mathur, B.L., Henry, J.: 'A novel fuzzy c-mean and s-transform method of discrimination and identification of inrush current in a power transformer', *J. Elect. Eng.*, 2010, **10**, pp. 16–23

[34] Wu, L., Liu, G., Tian, L.: 'Rapid harmonic detection based on generalized hs-transform'. 2014 IEEE Int. Conf. on Signal Processing, Communications and Computing (ICSPCC), Guilin, People's Republic of China, 2014, pp. 142–146

[35] Lobos, T., Sikorski, T., Wozniak, K.: 'Tracking of instantaneous spectrum components using time-frequency methods'. 2008 Conf. on Human System Interactions, Krakow, Poland, 2008, pp. 375–379

[36] Leonowicz, Z., Lobos, T., Wozniak, K.: 'Analysis of non-stationary electric signals using the s-transform', *COMPEL – Int. J. Comput. Math. Electr. Electron. Eng.*, 2009, **28**, (1), pp. 204–210

[37] Thangaraj, K., Muruganandham, J., Selvaumar, S., *et al.*: 'Analysis of harmonics using s-transform'. 2016 Int. Conf. on Emerging Trends in Engineering, Technology and Science (ICETETS), Pudukkottai, India, 2016, pp. 1–5

[38] Chu, H., Xie, D., Zhang, Y.: 'S-transform application in harmonic analysis of a DFIG-based wind energy conversion'. Electrical and Control Engineering & Materials Science and Manufacturing, Shanghai, People's Republic of China, 2016, pp. 169–174. Available at https://www.worldscientific.com/doi/abs/10.1142/9789813100312_0025

[39] Yao, W., Tang, Q., Teng, Z., *et al.*: 'Fast s-transform for time-varying voltage flicker analysis', *IEEE Trans. Instrum. Meas.*, 2014, **63**, (1), pp. 72–79

[40] Eghtedarpour, N., Farjah, E., Khayatian, A.: 'Effective voltage flicker calculation based on multiresolution s-transform', *IEEE Trans. Power Deliv.*, 2012, **27**, (2), pp. 521–530